Theoretical Study of the Oxidation of Phenolates by the [Cu2O2(N,N-di-tert-butylethylenediamine)2]2+Complex

ARTICLE *in* CHEMISTRY - A EUROPEAN JOURNAL · JANUARY 2013

Impact Factor: 5.73 · DOI: 10.1002/chem.201203052 · Source: PubMed

CHEMISTRY
A EUROPEAN JOURNAL

ChemPubSoc Europe

DOI: 10.1002/chem.201203052

VIP

Theoretical Study of the Oxidation of Phenolates by the $[Cu_2O_2(N,N'\text{-di-}tert\text{-butylethylenediamine})_2]^{2+}$ Complex

Yan Fang Liu,*[a, b] Jian Guo Yu,[a] Per E. M. Siegbahn,[b] and Margareta R. A. Blomberg*[b]

Abstract: Experiments have shown that the μ-η^2:η^2-peroxodicopper(II) complex $[Cu_2O_2(N,N'$-di-*tert*-butylethylenediamine$)_2]^{2+}$ rapidly oxidizes 2,4-di-*tert*-butylphenolate into a mixture of catechol and quinone and that, at the extreme temperature of −120 °C, a bis-μ-oxodicopper(III)−phenolate intermediate, labeled complex **A**, can be observed. These experimental results suggest a new mechanism of action for the dinuclear copper-containing enzyme tyrosinase, involving an early O−O bond-cleavage step. However, whether phenolate binding occurs before or after the cleavage of the O−O bond has not been possible to answer. In this study, hybrid density functional theory is used to study the synthetic reaction and, based on the calculated free-energy profile, a mechanism is suggested for the entire phenolate-oxidation reaction that agrees with the experimental observations. Most importantly, the calculations show that the very first step in the reaction is the cleavage of the O−O bond in the peroxo complex and that, subsequently, the phenolate substrate coordinates to one of the copper ions in the bis-μ-oxodicopper(III) complex to yield the experimentally characterized phenolate intermediate (**A**). The oxidation of the phenolate substrate into a quinone then occurs in three steps: 1) C−O bond formation, 2) coupled internal proton and electron transfer, and 3) electron transfer coupled to proton transfer from an external donor (acidic workup, experimentally). The first of these steps is rate limiting for the decay of complex **A**, with a calculated free-energy barrier of 10.7 kcal mol^{-1} and a deuterium kinetic isotope effect of 0.90, which are in good agreement with the experimental values of 11.2 kcal mol^{-1} and 0.83(±0.09). The *tert*-butyl substituents on both the phenol substrate and the copper ligands need to be included in the calculations to give a correct description of the reaction mechanism.

Keywords: copper · density functional calculations · oxidation · phenolates · reaction mechanisms

Introduction

The tyrosinase enzyme has a dinuclear copper active site, similar to that in hemocyanins and catechol oxidase, at which the reduced dicopper(I) reacts with O_2, thereby producing a side-on bridging μ-η^2:η^2-peroxodicopper(II) complex (Cu···Cu about 3.6 Å), which can perform phenol hydroxylation and oxygenation reactions, thus giving *o*-catechols or *o*-quinones (Scheme 1).[1]

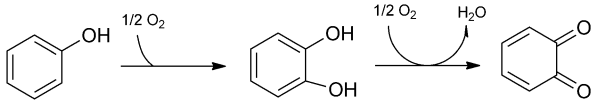

Scheme 1. Mechanism of phenol oxidation catalyzed by tyrosinase.

The hydroxylation of phenol by tyrosinase is complicated and the reaction mechanism is not yet fully understood. Several different mechanistic proposals have been put forward.[1b,f,n,2] The most accepted mechanism, based on both theory and experimental data, proposes that a μ-η^2:η^2-peroxide species performs the hydroxylation reaction through an electrophilic aromatic substitution reaction and that the cleavage of the O−O bond occurs either concerted with or after the C−O bond formation.[1b,f,n,2a,c,e] In one of the theoretical studies of the mechanism, the C−O bond was reported to form before O−O cleavage,[2b] whereas, in another one, the O−O bond was cleaved first.[2d] However, this latter result has been shown to be due to convergence to an incorrect local minimum.[2h]

Owing to the structural and functional complexity of enzymes, the synthesis of inorganic compounds to mimic their reactivity has become an important and efficient strategy for shedding light on their structural and spectroscopic properties, as well on as their reaction mechanisms.[3] To reproduce and understand the chemical reactivity of tyrosinase, a

[a] Dr. Y. F. Liu, Prof. J. G. Yu
College of Chemistry, Beijing Normal University
No. 19, XinJieKouWai St., HaiDian District
Beijing 100875 (P.R. China)
Fax: (+46) 8-55-37-86-01
E-mail: yanfang.liu@fysik.su.se

[b] Dr. Y. F. Liu, Prof. P. E. M. Siegbahn, Prof. M. R. A. Blomberg
Department of Physics and Department of Biochemistry
and Biophysics, Stockholm University
106 91 Stockholm (Sweden)
Fax: (+46) 8-55-37-86-01
E-mail: mb@fysik.su.se

Supporting information for this article is available on the WWW under http://dx.doi.org/10.1002/chem.201203052.

number of copper complexes have been synthesized, which perform the hydroxylation or oxidation of either an external substrate or of one of the copper ligands.[3e,f,i,o,4] Understanding the mechanism of biomimetic complexes should be helpful for mechanistic comparisons with enzymes and also for the design of more efficient catalysts that could have potential industrial applications.

Stack and co-workers reported the synthesis of a μ-η^2:η^2-[peroxodicopper(II)(DBED)$_2$]$^{2+}$ complex (DBED = *N*,*N*′-di-*tert*-butylethylenediamine), labeled P^{DBED}, which rapidly hydroxylated and oxidized 2,4-di-*tert*-butylphenolate to produce a mixture of catechol and quinone products upon acidic workup (Scheme 2).[4g,j,m] They showed that P^{DBED} contained a μ-η^2:η^2-peroxodicopper(II) species and a secondary diamine ligand of DBED, with an intact O–O bond and a Cu–Cu distance of 3.45 Å.[4g,j] In solution, the [Cu$_2$O$_2$(DBED)$_2$]$^{2+}$ complex existed as 95% μ-η^2:η^2-peroxodicopper(II) and 5% bis-μ-oxodicopper(III) before interaction with the phenolate substrate.[4g,j,m]

At −80 °C, P^{DBED} reacts with 2,4-di-*tert*-butylphenolate, without the appearance of any intermediate species, to yield a 1:1 mixture of *o*-catechol and *o*-quinone. However, it was also shown that a bis-μ-oxodicopper(III)–phenolate complex with a cleaved O–O bond (intermediate **A**) could be observed in solution at extremely low temperatures (−120 °C) and that this intermediate oxygenated the phenolate through two subsequently observed intermediates (**B** and **C**), where intermediate **C** appeared after the addition of an acid to the solution (Scheme 2).[4g,m] Based on the measured inverse secondary C–H/C–D isotope effect of 0.83(±0.09), it was proposed that the mechanism of the hydroxylation of species **A** has the hallmark of an electrophilic aromatic substitution mechanism, in which a carbon center undergoes a hybridization change from sp^2 to sp^3 in the transition state.[4g,m]

Thus, Stack and co-workers have shown that P^{DBED} is able to mimic the activity of tyrosinase (Scheme 2). The suggested phenol-hydroxylation mechanism, in which the formation of the C–O bond occurs after the cleavage of the O–O bond, presents an alternative to the late-stage O–O-cleavage mechanisms, in which the cleavage of the O–O bond occurs concerted with—or even after—the formation of the C–O bond, which was previously proposed for tyrosinase. However, the question of whether the O–O bond is cleaved before, concerted with, or after the binding of the phenolate substrate cannot be resolved by this experiment, because the μ-η^2:η^2-peroxodicopper(II) and the bis-μ-oxodicopper (II) isomers are in equilibrium at −80 °C.[4g,h,j]

Recently, Güell et al. used hybrid density functional theory (B3LYP) and a small model (in which the *tert*-butyl substituents in the experimental system were replaced by methyl groups on the copper complex and by hydrogen atoms on the substrate) to study the experimentally observed reactions of the P^{DBED} complex with phenolate.[5] The calculated energy profile supported the suggestion that a bis-μ-oxodicopper(III)–phenolate complex can perform the hydroxylation reaction, but it could not determine whether the peroxide O–O bond was cleaved before or after the association of the phenolate. In fact, the free-energy profile indicated that the experimentally observed bis-μ-oxodicopper-(III)–phenolate intermediate (**A**) would be easily and irreversibly converted into a very stable μ-η^2:η^2-peroxodicopper(II)–phenolate complex, which is in contrast to the experimental observations. Op′t Holt et al. used the same hybrid density functional (B3LYP) and a slightly larger model (which retained the *tert*-butyl substituents on the copper complex but used an unsubstituted phenolate substrate) to describe the experimentally observed intermediates (**A**, **B**, and **C**) and some aspects of the transitions between these intermediates.[4g,m] However, in that study, neither the cleavage of the O–O bond nor the substrate-binding step were addressed. Thus, none of these previous studies used the fully substituted chemical systems to calculate the entire phenolate-hydroxylation energy profile, starting with the peroxide P^{DBED} complex. Because this reaction is a redox process, the substituents, in particular those on the substrate, might affect the energetics of the electron-transfer steps, apart from any possible steric effects from the substituents on both the substrate and the copper complex. In terms of the methods used, it is also noted that none of these previous studies on the [Cu$_2$O$_2$(DBED)$_2$]$^{2+}$ complex included dispersion effects, which has recently been shown to be important when bulky ligands are involved.[6]

Because there were still several unresolved questions concerning the mechanism of this reaction, we decided to perform a comprehensive study of the reaction between the [peroxodicopper(II)(DBED)$_2$]$^{2+}$ complex (Figure 3) and a di-*tert*-butylphenolate substrate by using the fully substituted compounds. Our main objective was to shed further light on the initial reaction steps, that is, to try to determine at what stage the O–O bond is cleaved. As shown below, the results for this large model differ substantially in some parts of the potential-energy surface from those for the small model that

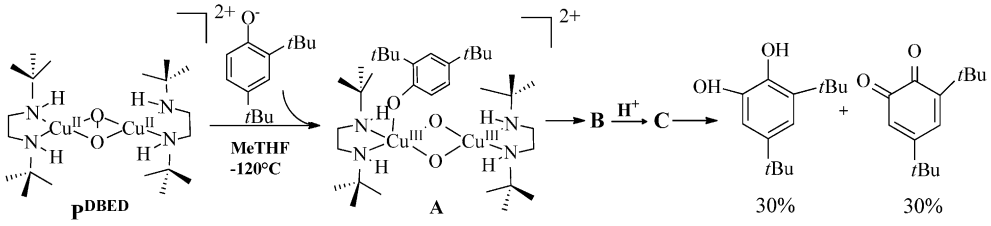

Scheme 2. Experimental results that were obtained by Stack and co-workers.[4g,j,m]

was used previously. To obtain a more complete picture, all of the steps that led to full oxidation of the substrate, that is, to the formation of the quinone, were also studied. Unlike the earlier studies, the modified Becke′s three-parameter exchange correlation potential with an exact exchange parameter value of 15% (B3LYP*) was used for the final results, as discussed below. Full optimization of all of the intermediates and the transition states were performed by applying both antiferromagnetic and ferromagnetic coupling of the spins of the two copper ions. Furthermore, our calculated results included solvent effects, dispersion corrections,[6a,b] and thermal and entropy corrections, which allowed for a direct comparison with experimental measurements. In this context, it is important to note that, since the earlier studies were performed, dispersion effects have been demonstrated to be quite important in this type of system.[6c] A particular difficulty in the study of this reaction is how to calculate the relative energy of association between the negatively charged phenolate substrate and the positively charged $[Cu_2O_2(DBED)_2]^{2+}$ complex in a reasonably accurate way, as already noted in the previous study by Güell et al.[5] Herein, a different approach is taken, which combines experimental and computational information to obtain a more reliable description of the substrate binding.

In a recent theoretical study, a similar reaction, namely the oxidation of catechol into *ortho*-quinone by a copper–bispidine complex, was investigated by using both energetic and spectroscopic parameters.[7] It can be noted that the main approach in the present study is to use energetics as a mechanistic probe, whilst spectroscopic parameters can also be useful, as shown in several previous studies.[4l,m,7–8]

Herein, by using the fully substituted chemical systems, which is a reliable method for describing substrate binding, and by including the dispersion effects that are missing in density functional theory, an energy profile is obtained that suggests a mechanism for the entire reaction that is in agreement with available experimental observations. The reaction, starting from the μ-η^2:η^2-peroxodicopper(II) complex (P^{DBED}, **1**) is initiated by the cleavage of the O–O peroxide bond into a bis-μ-oxodicopper(III) complex (**2**), followed by the direct coordination of the 2,4-di-*tert*-butylphenolate, thereby giving the experimentally observed bis-μ-oxodicopper(III)–phenolate (**3**). In agreement with previous suggestions, the bis-μ-oxodicopper(III)–phenolate (**3**) is shown to undergo an electrophilic aromatic substitution reaction for the formation of a C–O bond with one of the bridging oxygen atoms (**4**), followed by the transfer of a proton from the ring onto the other oxygen atom of the Cu_2O_2 core. The proton transfer is coupled to an electron transfer from the substrate to one of the copper ions (**5**). In the final step that was studied, the addition of an acid, which is modeled here as a protonation of the copper-bridging hydroxyl group, leads to dissociation into two mononuclear copper complexes with a quinone coordinated to one of the reduced Cu^I ions (**6**).

Computational Details

The calculations were performed by using unrestricted DFT with the B3LYP and B3LYP* hybrid density functionals.[9] It has been shown that the modified B3LYP* functional, in which 15% Hartree–Fock exchange is used instead of 20% (as in the original B3LYP functional), improves the performance of calculations on metal complexes in weak ligand fields.[9c,10] The accuracy of different DFT functionals was recently assessed in terms of the binding energy of the CuO^+ cation, where it was shown that B3LYP gave reasonably accurate results.[11] The electronic energy calculations in this study were performed in three steps: First, the geometries were optimized at the unrestricted B3LYP (UB3LYP)/lacvp* level by using Jaguar 7.0.[12] The lacvp* basis set, as implemented in Jaguar, is a standard double-ς basis set with polarization functions on all atoms except for hydrogen atoms and an effective core potential on the metal.[13] In the second step, accurate energies of the optimized structures were calculated at both the B3LYP and B3LYP* levels by using the cc-pVTZ(-f) basis set for all main-group atoms, which is a triple-ς basis set with polarization functions.[14] An effective core potential with a triple-ς basis set and diffuse functions, lacv3p*, was used to treat the metal. Finally, by using a self-consistent-reaction-field method implemented in Jaguar,[15] electrostatic solvation effects from the surrounding protein were calculated in the optimized structures with the lacvp* basis set. For the solvent methyltetrahydrofuran, a dielectric constant of 7.0 was used and the probe radius was set to 2.71 Å. Full transition-state optimizations and analytical Hessians (second derivatives of the energy with respect to the nuclear coordinates) for all of the stationary points were obtained by using the Gaussian 09 program[16] with the same functional and basis set as for the geometry optimizations in Jaguar. Hessians were used to determine the nature of each stationary point and to calculate zero-point energies, thermal corrections, and entropy effects. One general drawback of DFT is its inability to describe long-range electron correlations, which are responsible for attractive van der Waals forces.[6a,b] To improve the results, dispersion corrections (which were calculated by using the empirical formula of Grimme[6a,b]) were applied to the calculated energies. The final free energies given in this work include energies that were computed at the B3LYP*/cc-pVTZ(-f)&lacv3p*//B3LYP/lacvp* level of theory, together with solvent effects and dispersion corrections that were obtained with the B3LYP/lacvp* method, and thermal (including zero-point energies) and entropy corrections that were calculated by using the B3LYP/lacvp* method at −120 °C. The decision to use the B3LYP* energies as the main results, rather than the B3LYP energies, is commented on below. The main difference between these two functionals concerns the relative energies in cases that involve one closed-shell state and one open-shell state with unpaired electrons, for which the amount of exact exchange has a large effect. As discussed below, for a couple of situations, comparison with experimental results shows significantly better agreement for the B3LYP* values. A comparison between B3LYP and B3LYP* for all stationary points along the reaction path is given in the Supporting Information, Table S1. As mentioned in the Introduction, both antiferromagnetic and ferromagnetic coupling of the unpaired spins on the complex are investigated. In most cases, only the results for the lowest spin-state are reported, whilst, in a few interesting cases, different spin-states for the same intermediate are discussed.

The fully substituted chemical systems were used in the calculations. Each of the four nitrogen atoms that coordinate the copper atoms is bound to one hydrogen atom and one *tert*-butyl group that can be oriented in different ways, thereby resulting in many different conformations of the dimeric complex. From the available experimental information, it does not seem possible to exclude any of those conformations. Therefore, an investigation was performed that compared the relative energies of the different conformations in several intermediates in the reaction studied. As it turned out, the conformation with the lowest energy for the reactant was also the lowest, or very close to the lowest one, for the most important intermediates and transition states. Therefore, only the results for this conformation are reported herein. In one case, for intermediate **2′**, a significantly more stable conformation was found, but this conformation was found to be surrounded by even higher barriers

than those reported below for the main conformation. Therefore, this conformation of structure **2′** cannot be involved in the reaction and, hence, it is not discussed further.

Cartesian coordinates for the most important structures are provided in the Supporting Information. Also, a comparison of the geometrical parameters and spin populations from this work with the results from previous studies is given in the Supporting Information.

Results and Discussion

Our quantum-chemical calculations start with the peroxo form of the $[Cu_2O_2(DBED)_2]^{2+}$ complex (**1**, Figure 1), which is the predominant form found experimentally.[4g] In this complex, each copper(II) ion forms a planar four-coordinated complex and O_2 is bound in a side-on bridging fashion (Figure 1 and the Supporting Information, Table S2). Two different spin states were optimized: The antiferromagnetically coupled (open-shell) singlet state and the ferromagnetically coupled triplet state. The singlet state was found to be slightly lower than the triplet state. The optimized Cu–Cu distance (3.63 Å) is somewhat longer than the experimental value of 3.45 Å, but similar distances were found for the singlet state in previous computational studies (see the Supporting Information, Table S2).[4g,5]

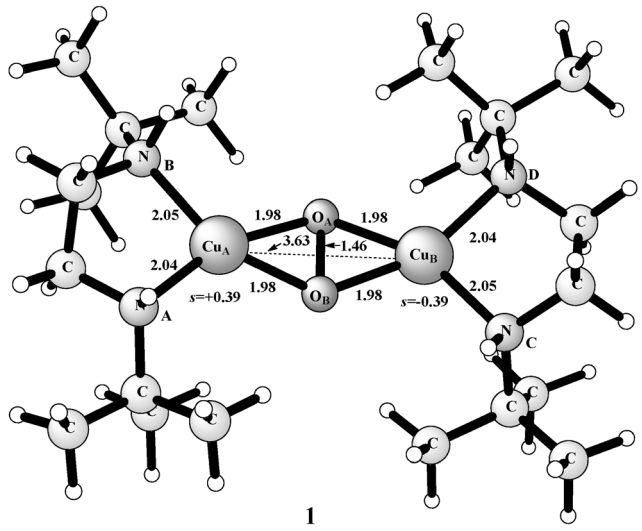

Figure 1. Synthetic μ-η^2:η^2-peroxodicopper(II) complex reported by Stack and co-workers[4g] and the optimized structure that was obtained in this study (**1**, open-shell singlet); selected distances [Å] are indicated, as are the most important spin populations.

The reaction of peroxodicopper(II) complex **1** with the phenolate substrate can be divided into two parts. The first part concerns the binding of the substrate to the copper complex and the O–O-cleavage step, with oxidation of both Cu^{II} ions into Cu^{III}, thus yielding the experimentally observed (and rather well-characterized) bis-μ-oxo phenolate complex (**A**). This part of the reaction (**1**→**3**) is described in the first subsection below. In the second subsection, a series of subsequent steps (**3**→**6**), in which the phenolate substrate is oxidized into a quinone and the Cu^{III} ions are reduced to Cu^{I}, are described. The calculated free energies for the entire reaction mechanism studied in this work are shown in Figure 2.

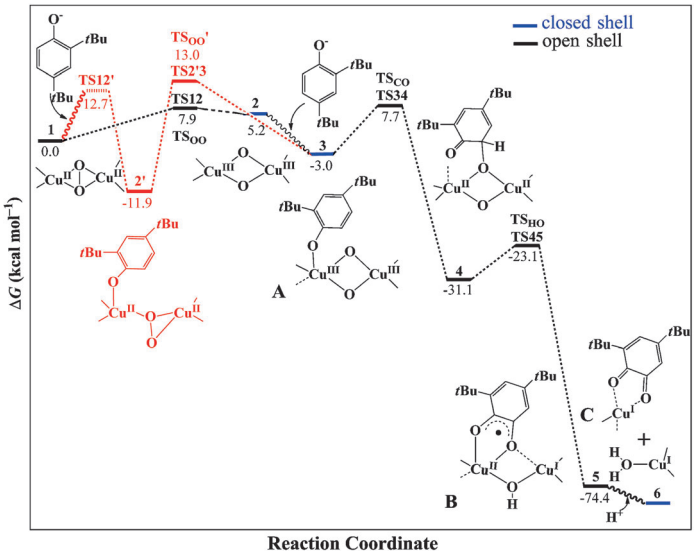

Figure 2. Calculated free-energy profile at −120 °C at the B3LYP* level of theory. The relative energies (*G*, in kcal mol^{-1}) are relative to structure **1** plus a phenolate. The copper ligands are removed for clarity.

Substrate binding (1→3): One crucial remaining question for understanding the detailed mechanism of the hydroxylation of 2,4-di-*tert*-butylphenolate by peroxide P^{DBED} concerns the nature of the phenolate-binding $[Cu_2O_2(DBED)_2]^{2+}$ complex. There are two different mechanistic possibilities (Scheme 3): In the first one (**1**→**2**→**3**), cleavage of the O–O bond occurs before the binding of the phenolate

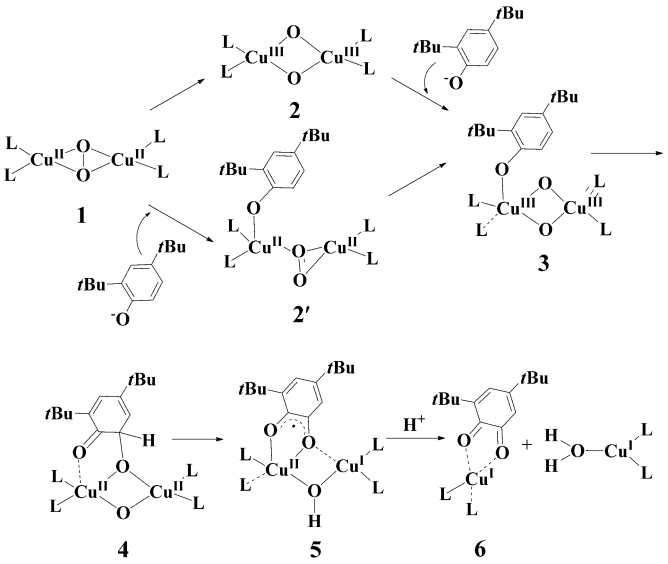

Scheme 3. Two possible reaction pathways that were investigated for the P^{DBED} complex (**1**).

substrate to the complex, whereas, in the second one (**1**→**2′**→**3**), cleavage occurs after the interaction of the substrate with the complex. Because the reaction involves the combination of two charged fragments (the negatively charged phenolate and the positively charged copper complex), it is difficult to calculate the relative energies for those steps and a purely computational distinction between the two mechanisms would require more explicit investigations of the solvent effects than what can be obtained by using the present continuum dielectric method. However, by combining the computational results with the experimentally determined binding constant, a picture of the entire reaction mechanism can be obtained (see below), as depicted in Figure 2.

Starting from peroxo complex **1**, the transition state for O–O cleavage (**TS12**) and the intermediate bis-μ-oxo form (**2**) were optimized (Figure 3 and the Supporting Information, Table S3). The barrier for this step was calculated to be 7.9 kcal mol^{-1} relative to complex **1**, and structure **2** is 5.2 kcal mol^{-1} higher than complex **1** (Figure 2). This low barrier indicates that the peroxo complex can easily transform into its bis-μ-oxo form and that the peroxo and bis-μ-oxo isomers are in equilibrium at low temperatures.[4g,h,j,5] The calculated relative energy for the bis-μ-oxo complex (+5.2 kcal mol^{-1}) is a few kcal mol^{-1} too high; rather, it should be about 1 kcal mol^{-1} higher than complex **1** to agree with the detection of 5% of the complex as its bis-μ-oxo form at −80 °C by Mirica et al.[4g] However, it should be noted that peroxo complex **1** is an open-shell singlet state with two unpaired electrons and that bis-μ-oxo complex **2** is a closed-shell state, which makes the calculated relative energy between them quite sensitive to the amount of exact exchange in the DFT functional, as illustrated by the fact that the corresponding B3LYP (20% exact exchange) value, +10.7 kcal mol^{-1}, is much higher than the B3LYP* (15% exact exchange) value, +5.2 kcal mol^{-1}. Therefore, the agreement with experiment has to be considered as reasonably good for the B3LYP* functional, which is also the reason for using the relative energies that were obtained with this functional as the main results in this investigation. In 2009, Güell et al.[5] also investigated this reaction step by using the small model, in which the *tert*-butyl substituents in $[Cu_2O_2(DMED)_2]^{2+}$ are replaced by methyl groups. The main difference, compared to our results, is that they obtained a relative free energy of complex **2** compared to complex **1** of −2.5 kcal mol^{-1}. This value was obtained by using the B3LYP functional and without including dispersion effects. With dispersion effects included and using the B3LYP* functional, a value of −9.5 kcal mol^{-1} was obtained for the small model, which is significantly different from the value of +5.2 kcal mol^{-1} that we obtained for the large model. The reason for this large difference in relative energy can be easily understood by considering the geometries of optimized isomers **1** and **2**. The shorter Cu–Cu distance in the bis-μ-oxo complex (**2**, 2.87 Å; Figure 3) compared to that in the peroxo complex (**1**, 3.63 Å; Figure 1) makes the repulsive effects of the bulky ligands in the large model much larger in complex **2** than in complex **1**, thus destabilizing

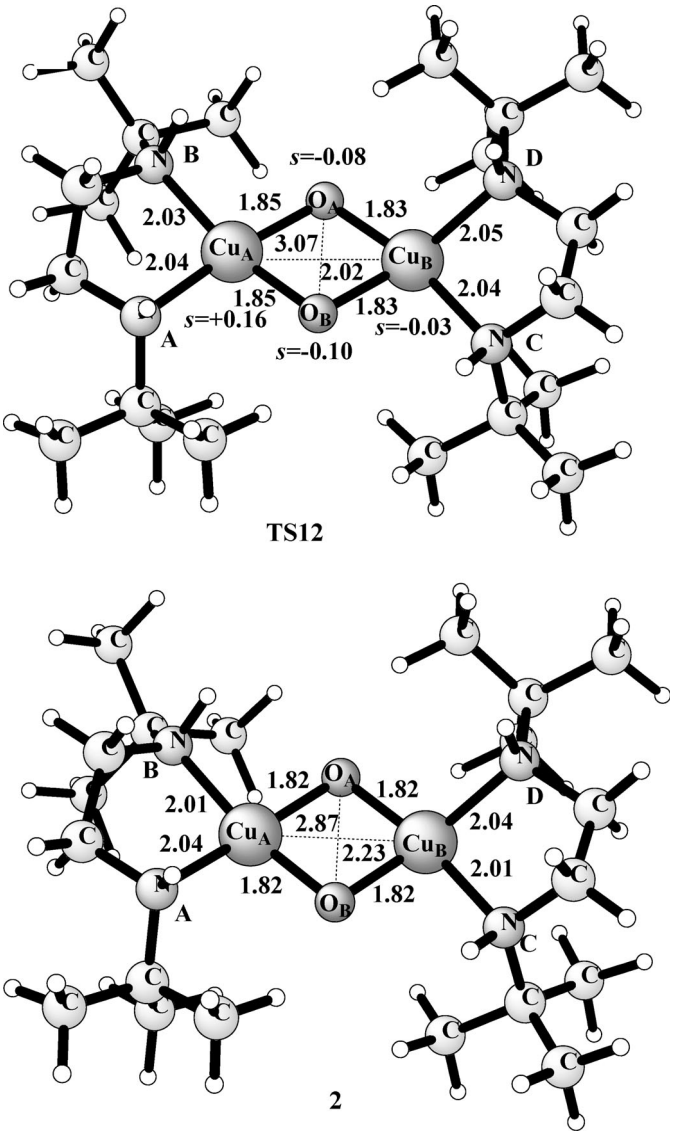

Figure 3. Optimized structures of the O–O bond-cleavage transition state (**TS12**, open-shell singlet) and the bis-μ-oxo complex (**2**, closed-shell singlet); selected distances [Å] are indicated, as are the most important spin populations.

complex **2** relative to complex **1** when going from the small to the fully substituted model.

The next step is to investigate the binding of the 2,4-di-*tert*-butylphenolate to the copper complex, either to structure **2**, which would lead directly to structure **3** (a bis-μ-oxo complex in which the phenolate is bound to one of the copper ions), or to peroxide complex **1**, which would lead to structure **2′** and which would require an O–O-cleavage step before structure **3** is reached (Scheme 3). As mentioned above, the relative energy of binding the negatively charged phenolate to the positively charged copper complex cannot be accurately calculated by using the presently available methods. The explicitly calculated relative energy by using the pcm method, in the same manner as in reference [5], is −15.8 kcal mol^{-1}, which is quite similar to the corresponding

value in reference [5] ($-18.8\,kcal\,mol^{-1}$). Both of these values are quite unrealistic; therefore, instead, we used the experimentally determined binding constant for complex **A** ($16000\,M^{-1}$) that was obtained from optical titrations of P^{DBED} with sodium 2,4-di-*tert*-butylphenolate at 153 K.[4m] This experimental value implies that complex **A** is 2.9 kcal mol^{-1} more stable than the reactant complex and, therefore, we placed optimized structure **3** at $-3\,kcal\,mol^{-1}$ in the energy profile, by taking the peroxo complex as the reference (Figure 2). Thus, the two parts of the energy profile, that is, with and without the phenolate, are merged together in a way that is more reliable than using the directly calculated continuum solvent effects.[5]

Adding the 2,4-di-*tert*-butylphenolate substrate to bis-μ-oxo complex **2** leads to the formation of intermediate **3** (Figure 4) without any barrier. This intermediate, in which

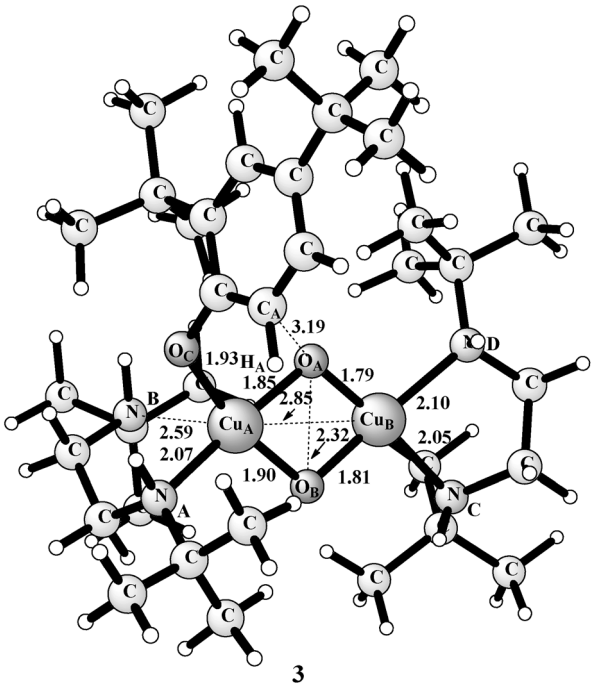

3

Figure 4. Optimized structure of a phenolate-bonded bis-μ-oxodicopper-(III) species (**3**, closed-shell singlet); selected distances [Å] are shown. Intermediate **3** is thought to correspond to experimentally observed complex **A**.

the 2,4-di-*tert*-butylphenolate substrate is bound to the bis-μ-oxodicopper(III) core, supported by the DBED ligand, corresponds to experimentally observed compound **A**. The ground state is a closed-shell singlet state (for selected parameters of the optimized structure, see Figure 4 and the Supporting Information, Table S4). In the Cu_2O_2 core, the Cu–Cu and O–O distances (2.85 and 2.32 Å, respectively) are typical of a bis-μ-oxodicopper(III) structure. The Cu–O bond lengths vary between 1.80 and 1.90 Å. Cu_B is bound to DBED with Cu–N bond lengths of 2.05 and 2.10 Å, whereas the 2,4-di-*tert*-butylphenolate-bonded Cu_A atom exhibits a similar Cu–N distance to its remaining diamine ligand, with Cu_A–N bond lengths of 2.07 Å. The second Cu_A–N bond increases to 2.59 Å as this ligand is replaced by the 2,4-di-*tert*-butylphenolate oxygen atom, with a distance to the Cu_A atom of 1.93 Å. This structure corresponds well to the experimentally observed structure (**A**), in which the distance between the two copper ions is 2.79 Å and the average distance between each copper atom and the four nitrogen/oxygen ligands is 1.89 Å.[4g] Previously, Stack and co-workers[4g,m] and Güell et al.[5] used smaller models to optimize a structure that corresponded to our structure **3** and they obtained geometrical parameters that were quite similar to those found in this study (see the Supporting Information, Table S4).

In spite of the similarities between the previous and present results (see above) for intermediate **3**, we found that the properties of this intermediate strongly depended on the chemical model and also, to some extent, on the density functional that were used. In fact, for several intermediates in this reaction, the fully substituted 2,4-di-*tert*-butylphenolate substrate facilitates electron transfer from the substrate to the copper ions, unlike the unsubstituted phenolate model used in previous studies.[4m,5] Therefore, by using the fully substituted chemical system in these calculations on intermediate **3**, another low-lying state (**3′**; see the Supporting Information, Figure S1), which is an open-shell singlet state with two unpaired electrons, is also obtained. This state has a long distance between the phenol oxygen and copper atoms, a substrate radical, and one extra electron that is delocalized over the Cu_2O_2 core (see the spin population in the Supporting Information, Figure S1) compared to the closed shell Cu^{III},Cu^{III} state (Figure 4). In fact, by using the B3LYP functional, the open-shell state with an oxidized substrate is the ground state, about 5 kcal mol^{-1} lower than the closed shell state. On the other hand, with only 15% exact exchange, as in the B3LYP* functional, the two states of intermediate **3** have the same energy. Because the structural properties of the closed-shell state agree with the experimental observations, we conclude that this state should be the ground state. This result provides further motivation for mainly reporting the B3LYP* results rather than the B3LYP results in this study. By using the small-substrate model, no electron transfer from the substrate to the copper ions occurs in the calculations and only the closed-shell state of intermediate **3** plays a role. Obviously, if only the closed-shell state of intermediate **3** is investigated, the structure that corresponds to the experimental structure would be obtained by using any model. It could be argued that the small unsubstituted phenol is a good model of the experimentally used 2,4-di-*tert*-butylphenolate substrate at this stage of the reaction, because the correct structure is obtained by using this model. However, as will be seen below, the state with an oxidized substrate, which is only found for the large model, plays a role in creating high barriers that avoid the low-lying (but unobserved) intermediate **2′**.

To probe the second pathway (Scheme 3), we also optimized complex **2′**, which contained an intact O–O peroxo

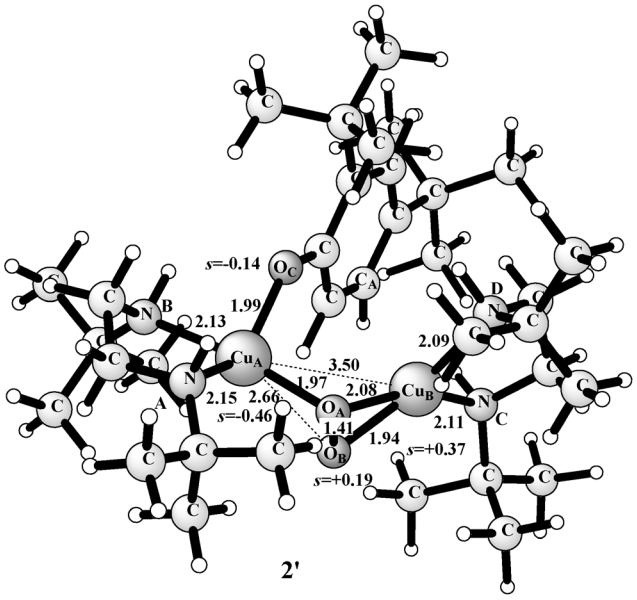

Figure 5. Optimized structure of a phenolate-bonded peroxodicopper(II) intermediate (**2′**, open-shell singlet); selected distances [Å] are indicated, as are the most important spin populations.

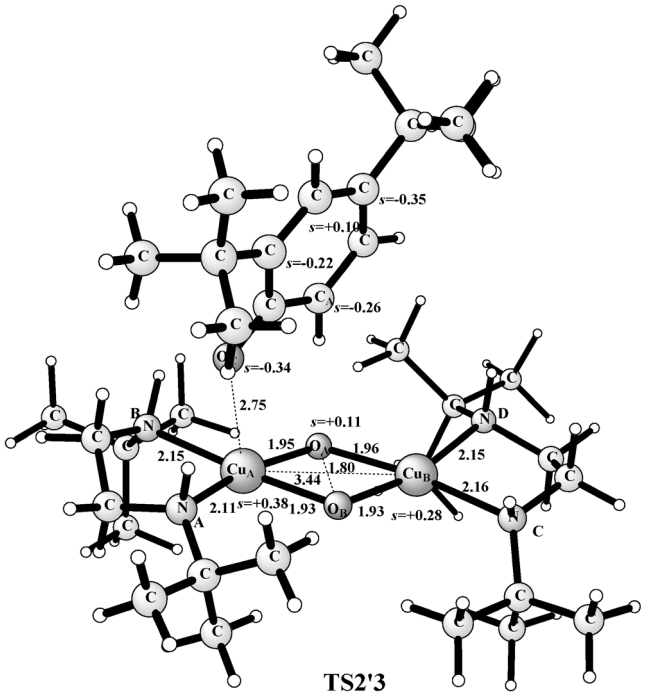

Figure 6. Optimized structure of the transition state for O–O bond cleavage (**TS2′3**, open-shell triplet); selected distances [Å] are indicated, as are the most important spin populations.

bond and a phenolate that was bound to one of the Cu ions (Figure 5). This complex was found to be 8.9 kcal mol^{-1} lower in energy than complex **3**, in which the O–O bond had been cleaved (Figure 2). This result is similar to what was found in reference [5]. In that study, it was difficult to explain why complex **3** and not complex **2′** was observed experimentally, because no barrier was found between structures **1** and **2′** and the barrier from complex **3** to complex **2′** was quite low (only 9.6 kcal mol^{-1}). On the other hand, in this study, high barriers were actually found that prevent the formation of stable complex **2′**. On moving from complex **3** to complex **2′**, the barrier (**TS2′3**) was found to be 16.0 kcal mol^{-1}, which effectively stopped this reaction step from occurring. Furthermore, this barrier was as much as 5.3 kcal mol^{-1} higher than the computed forward barrier from complex **3** (see below). The structure of the lowest transition state, **TS2′3** (Figure 6), was quite different in this study compared to the corresponding lower transition state by using a small model.[5] As shown in Figure 6, the state with an oxidized substrate (see above) is involved in this transition state. In fact, as can be seen from the more detailed energy profile in the Supporting Information (Figure S2), intermediate **3** first passes over a low barrier into its isoergonic form (**3′**), which contains a radical on the substrate, and then proceeds via transition state **TS2′3** into complex **2′**. The transition state from complex **3** to complex **2′** (which does not contain a radical on the substrate), which was found to be fairly low in energy for the small model used in reference [5], becomes much higher when the full model is used, owing to steric effects from the bulky ligands (see the Supporting Information, Figure S2). Furthermore, we found that there was also a rather high barrier for the direct binding of the phenolate to peroxide complex **1**, whereas, when using the small substrate model, there was no barrier for this reaction step.[5] This barrier is caused by the initial formation of a phenyl radical by electron transfer from the phenolate to the copper complex as they approach each other. As mentioned above, by using the small substrate model, electron transfer from the substrate to the copper ions does not occur and, therefore, this barrier does not appear. A structure with an oxidized substrate is located at 12.7 kcal mol^{-1}, by using this procedure to connect the two parts of the energy profile. This barrier, **TS12′**, has not been fully determined, but it is most likely more than 13 kcal mol^{-1}, that is, more than 5 kcal mol^{-1} higher than the barrier for cleavage of the O–O bond in transition state **TS12**.

To summarize, the initial reaction step in the hydroxylation of phenolate in the experiment by Stack and co-workers[4g,m] should be the binding of the phenolate to the O–O-cleaved bis-μ-oxo complex (**2**); this reaction step was found to occur without any barrier (see the energy profile, Figure 2) and yielded the observed complex **A** (**3**). Owing to high barriers (**TS12'** and **TS2′3**), it seems not to be possible to reach the very stable complex **2′** and the inaccessible pathway that proceeds through this complex has been colored red in the energy profile. Moreover, these conclusions depend on the use of the fully substituted chemical systems in the calculations and also on our procedure of combing the computational results with the experimental binding constant for the substrate.

Substrate oxidation (3→6): After the phenolate substrate is bound to the copper complex, thus giving intermediate **3**,

the oxidation of the substrate is initiated by the formation of a C–O bond (Scheme 3). The attack on the phenolate ring by one of the oxygen atoms in the Cu_2O_2 core destroys the aromaticity of the phenolate and, in the transition state, spin density appears on both the substrate ring and on the copper ions, which corresponds to the initiation of electron transfer from the substrate to the copper ions (Figure 7 and

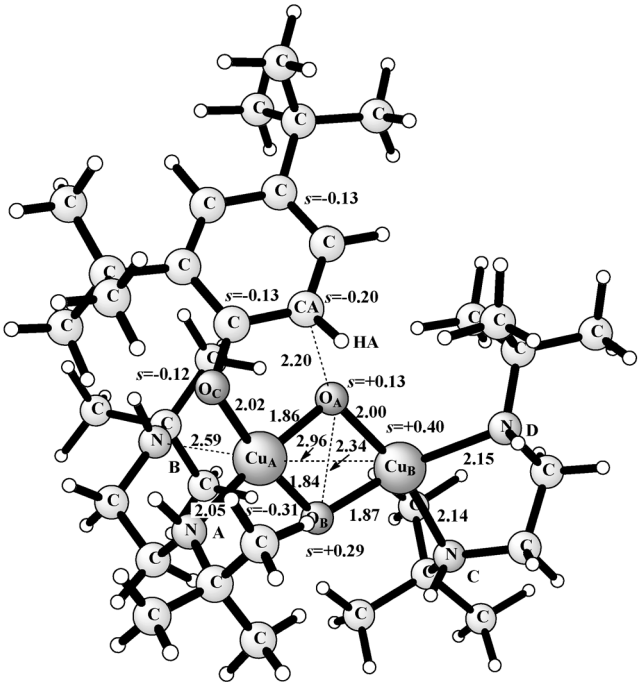

TS34

Figure 7. Optimized structure of the transition state for C–O bond formation (**TS34**, open-shell singlet); selected distances [Å] are indicated, as are the most important spin populations.

the Supporting Information, Table S5). Transition state **TS34** was located for the open-shell singlet state with two unpaired electrons. The structure for transition state **TS34** is shown in Figure 7 and it gives a free-energy barrier of 10.7 kcal mol^{-1}, which is in excellent agreement with the experimental value of 11.2 kcal mol^{-1} that was obtained from the lifetime of compound **A** at −120 °C.[4g] From this transition state, another bis-μ-oxo complex (**4**) is obtained, in which the phenol is two-electron oxidized and the two copper atoms are reduced back to Cu^{II}. The newly formed C–O bond has a distance of 1.39 Å (Figure 8), with an energy that is 28.1 kcal mol^{-1} lower than that of complex **3**. Structure **4** is not observed experimentally, but, from kinetic studies of the thermal-decay rates at −105 °C for complex **A** that is formed with 6-*d*-2,4-di-*tert*-butylphenolate and 6-*h*-2,4-di-*tert*-butylphenolate, a kinetic isotope effect (KIE) of 0.83(±0.09) was determined. By using our optimized transition-state structure (**TS34**), we obtained a KIE of 0.90 at −105 °C for step **3**→**4**, which agrees very well with the ex-

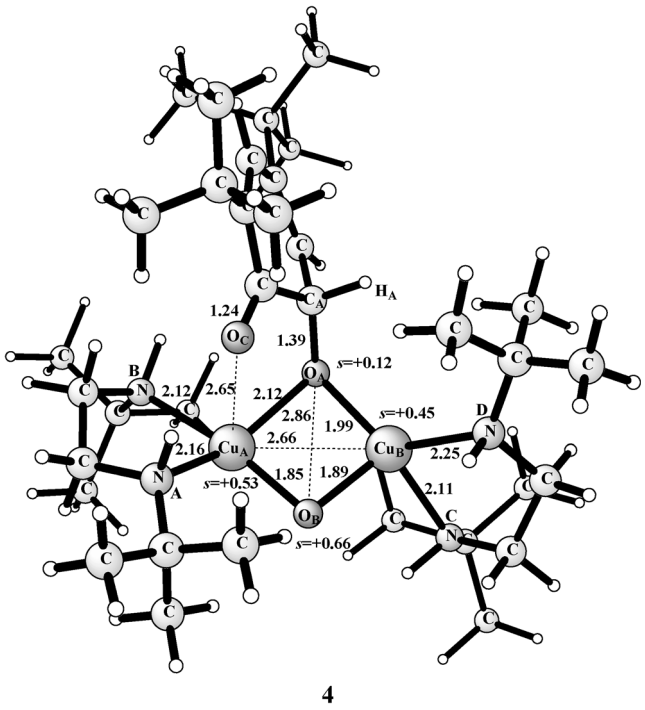

4

Figure 8. Optimized structure of the bis-μ-oxo complex (**4**, open-shell triplet); selected distances [Å] are indicated, as are the most important spin populations.

perimental value, thus indicating that this step is the rate-limiting step for the decay of intermediate **A**. Furthermore, such an inverse KIE indicates that the decay of intermediate **A** has the properties of an electrophilic aromatic substitution reaction, which is in agreement with the character of transition state **TS34**, in which carbon atom C_A undergoes a hybridization change from sp^2 to sp^3, as suggested in the experimental paper.[4g] In this step (**3**→**4**), the Cu_A–N_B distance decreases from 2.59 to 2.12 Å, whereas the Cu_A–O_C distance increases from 1.93 to 2.65 Å (Figure 4 and Figure 8).

Our calculated free-energy barrier for the transformation of complex **3** into complex **4** (10.7 kcal mol^{-1}) can be compared to the corresponding value obtained by Güell et al. (7.2 kcal mol^{-1}) by using a smaller model complex[5] and with the value obtained by Op't Holt et al. (4.5 kcal mol^{-1}) by using an intermediate model and a more approximate computational procedure.[4m] Several factors contribute to the differences in the calculated height of this barrier, apart from the model size, such as the choice of functional used, whether dispersion effects are included, etc. However, the calculated values of the KIE based on these reports, 0.88[5] and 0.90,[4m] respectively, show that the character of the transition state is correctly reproduced in all of the model calculations.

The next step in the phenolate-oxidation process is moving hydrogen atom (proton) H_A from the ring onto bridging oxygen atom O_B. The direct proton transfer to atom O_B in this system is different from the suggestion of

Op′t Holt et al.[4m] They argued that heterolytic cleavage of the C–H bond requires a driving force and that the long distance between the *ortho*-H and O_B atoms would not allow for a direct proton transfer. Therefore, they introduced an exogenous base to facilitate cleavage of the C–H bond, followed by the protonation of O_B.[4m] However, in this study, no exogenous base is needed. During the proton-transfer process, the O_B–H_A distance shortens from 4.35 Å in structure **4** to 0.97 Å in structure **5** (Figure 10 and the Supporting Information, Table S6). The ring of the substrate recovers aromaticity and the C_A carbon atom undergoes a hybridization change from sp^3 to sp^2. For this step, the triplet state (**TS45**, Figure 9) yields a barrier of 8.0 kcal mol^{-1} (Figure 2).

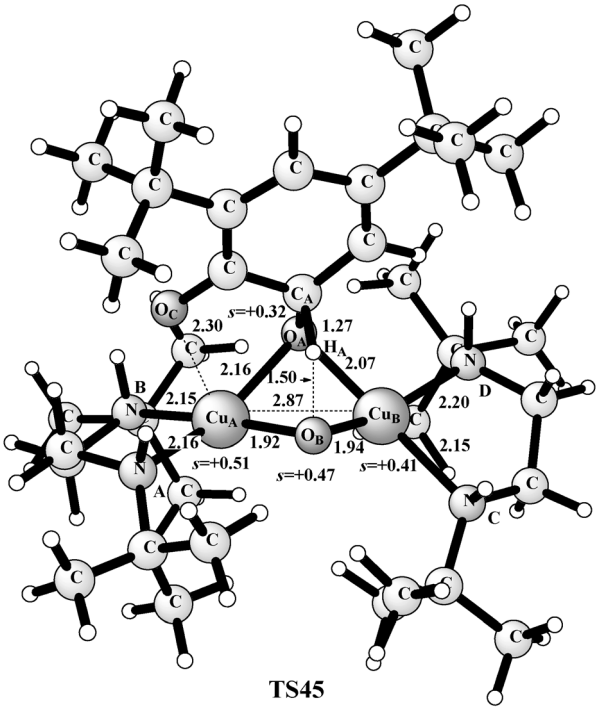

Figure 9. Optimized structure of the transition state for hydrogen-atom-transfer (**TS45**, open-shell triplet); selected distances [Å] are indicated, as are the most important spin populations.

Thus, the transfer of the hydrogen atom can be fast, which is the reason why structure **4** cannot be observed and also why the previous step (**3**→**4**), with a calculated barrier of 10.7 kcal mol^{-1}, is the rate-limiting step for the decay of complex **A** (**3**), in accordance with experimental observations. A direct proton transfer from the substrate to atom O_B with a low barrier was found also in the study by Güell et al.[5]

Proton transfer to oxygen atom O_B produces complex **5** (Figure 10) with an open-shell singlet energy that is 6.2 kcal mol^{-1} lower than the triplet state. In both the singlet and triplet states, a radical appears on the ring after the proton transfer (see the Supporting Information, Table S7) and the spin on atom Cu_B disappears, thus indicating that the proton transfer is coupled to an electron transfer from the substrate

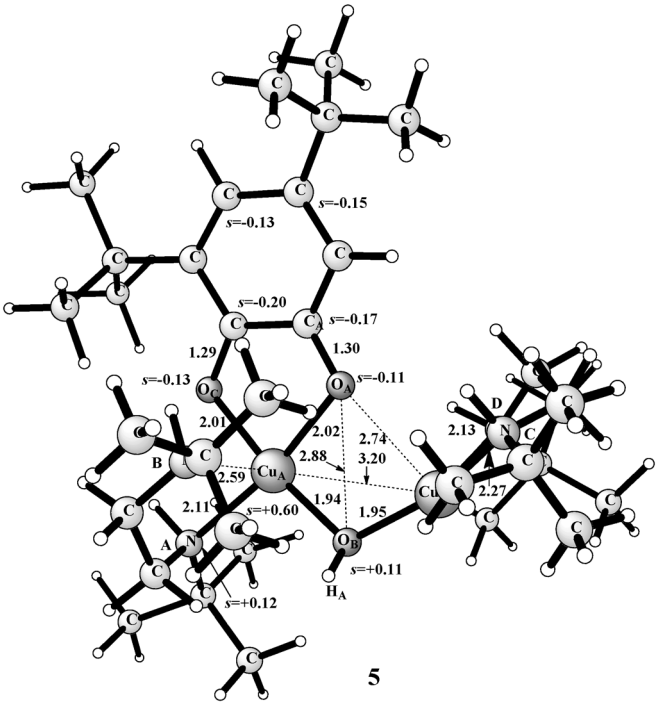

Figure 10. Optimized structure of a semiquinone–dicopper species with one Cu^{II} center and one Cu^{I} center (**5**, open-shell singlet); selected distances [Å] are indicated, as are the most important spin populations. Intermediate **5** is thought to correspond to experimentally observed complex **B**.

to Cu_B. Thus, in this step, the substrate has been one-electron oxidized and Cu_B has been reduced to Cu^{I}, which leads to an asymmetrically bonded semiquinone–dicopper species with one Cu^{II} atom and one Cu^{I} atom (Figure 10). In the experiment by Op't Holt et al.,[4m] an intermediate (**B**) was detected and, based on DFT calculations, they suggested that it (intermediate **B**) should correspond to the complex that forms after the protonation of the bridging oxygen atom (O_B), that is, to intermediate **5** in this study. However, Op′t Holt et al.[4m] claim that compound **B** is a catecholate with two Cu^{II} ions, which would mean that no electron transfer occurs from the substrate to Cu when the bridge is protonated. Herein, it was not possible to obtain a state with two Cu^{II} ions and a catecholate form of the substrate by using the large chemical system, thus indicating that the Cu^{II},Cu^{II} state is higher in energy. However, by using the small model from the study by Güell et al.,[5] it could be determined that, for the small model, the two states are close in energy, with the Cu^{II},Cu^{II} state ($_{SM}$**5′**) slightly lower than the Cu^{II},Cu^{I} state ($_{SM}$**5**, Figure 11 and Figure 12). These results are in line with the results discussed above for intermediate **3**, that is, that the fully substituted 2,4-di-*tert*-butylphenolate substrate facilitates electron transfer from the substrate to the copper ions more than the small unsubstituted phenolate model that was used in previous studies.[4m,5] Based on these results, we estimated that, for the fully substituted chemical system, the Cu^{II},Cu^{II}-catecholate state of complex **5** should be significantly higher in energy than the Cu^{II},Cu^{I}–semiquinone

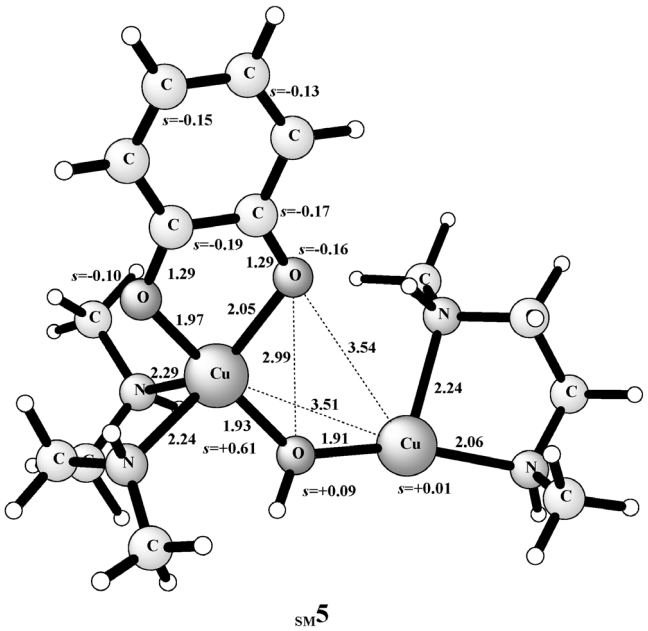

$_{SM}$**5**

Figure 11. Optimized structure of intermediate **5** by using the small model from ref. [5] ($_{SM}$**5**, open-shell singlet, see text); selected distances [Å] are indicated, as are the most important spin populations.

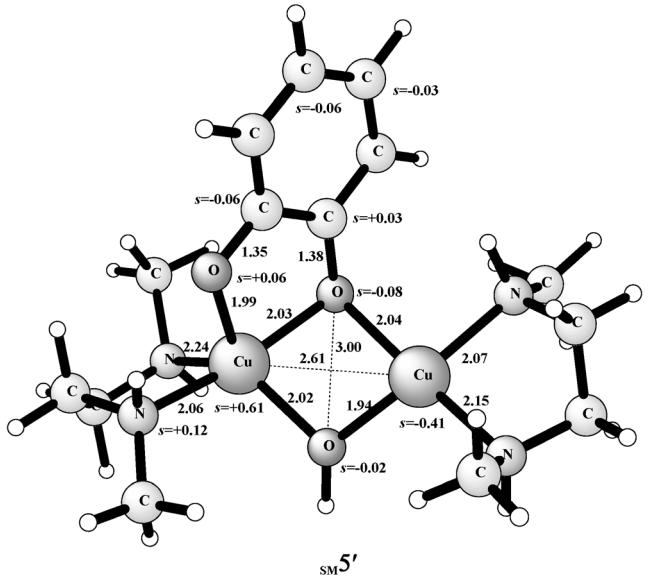

$_{SM}$**5′**

Figure 12. Optimized structure of intermediate **5** by using the small model from ref. [5] ($_{SM}$**5′**, open-shell singlet, see text); selected distances [Å] are indicated, as are the most important spin populations.

state. We conclude that one-electron oxidation of the substrate occurs in this step, thereby yielding an intermediate (**5**) that contains a semiquinone, one Cu^{II} ion, and one Cu^{I} ion and that this form of complex **5** most likely corresponds to experimentally observed intermediate **B**. The singlet ground state that was obtained for complex **5** was in agreement with the observation that intermediate **B** is EPR silent.

Notably, the intermediate that was obtained from the calculations by Op′t Holt et al.[4m] that corresponded to complex **5** was assigned to be a catecholate with two Cu^{II} ions, whereas the experimentally reported structure is very similar to that obtained for the semiquinone state ($_{SM}$**5**, Figure 11). Because no population analysis was reported in reference [4m] to support the assignment of the electronic structure, it seems likely that the state that was obtained in those calculations by using an unsubstituted substrate was actually the semiquinone state. As mentioned above, by using the small model, the two states are close in energy and, in fact, considering only the electronic energy, as in reference [4m], the semiquinone state is the lowest.

The last step in the reaction consists of the addition of one proton to the system, which corresponds to the addition of an acid in the experiment;[4m] in turn, this addition corresponds to the recovery of the tyrosine proton that is missing in the experiment with a phenolate substrate as compared to the enzymatic reaction. As suggested by Op′t Holt et al.,[4m] the addition of a proton to the hydroxy bridge in complex **5** results in the dissociation of a diamine–Cu^{I}–OH_2 monomer from the dimer. The remaining copper monomer was described as a Cu^{II}–semiquinone and should correspond to experimentally observed compound **C**.[4m] In this study, the second copper complex has two different states that are very close in energy: The lowest-energy state is obtained for a closed-shell singlet structure (**6**, Figure 13), which corresponds to a quinone-bound Cu^{I}–diamine complex (thus, the substrate is fully oxidized). The fact that the two states are so similar in energy makes it difficult to judge which of them corresponds to the experimentally observed compound

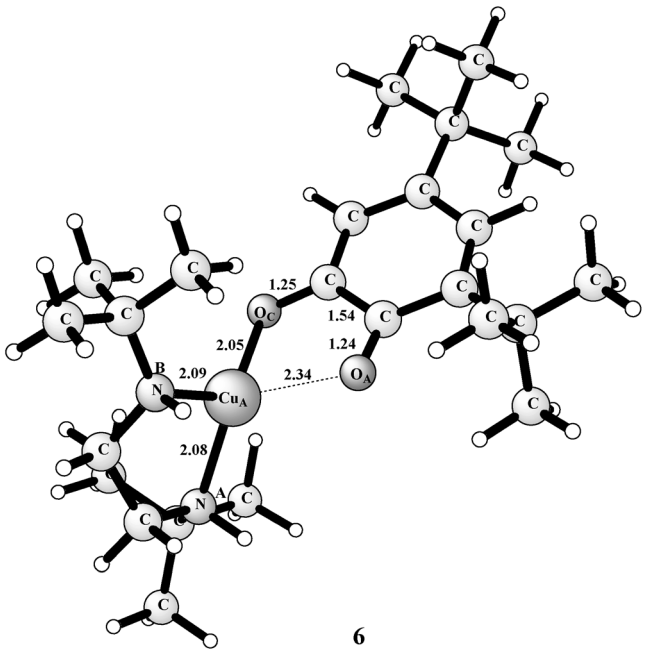

6

Figure 13. Optimized structure of a Cu^{I}–quinone (**6**, closed-shell singlet); selected distances [Å] are indicated. Intermediate **6** is thought to correspond to experimentally observed complex **C**.

(**C**). However, unequal isotope shifts in the resonance Raman spectra of complex **C** have been noted, which indicate that its experimental structure contains unequal Cu–O bond lengths.[4m] This observation indicates that compound **C** should correspond to the fully oxidized quinone and not to the semiquinone (cf. structures **6** and **6′**, Figure 13 and Figure 14). This assignment of the observed complex (**C**) is

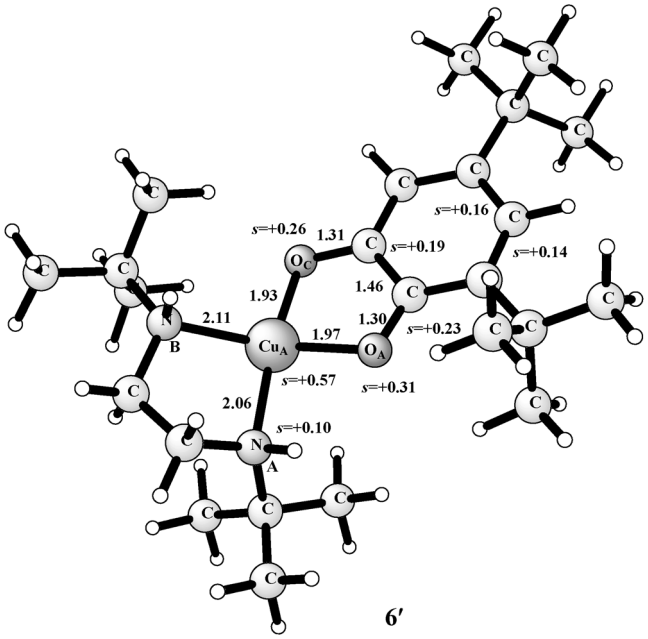

Figure 14. Optimized structures of a Cu^{II}–semiquinone (**6′**, triplet); selected distances [Å] are indicated, as are the most important spin populations. Intermediate **6** is thought to correspond to experimentally observed complex **C**.

at odds with the assignment made by Op′t Holt et al.,[4m] who suggested that the final state is a Cu^{II} complex with a semiquinone. In fact, their reported optimized structure for complex **C**, which contained very similar Cu–O bond lengths, corresponds to the structure for the Cu^{II} form without oxidation of the substrate (**6′**, Figure 14). As can be seen from the calculations on the two different states of complex **6**, the experimentally observed unequal Cu–O bond lengths do not stem from steric effects of the substituents on the substrate, as argued in reference [4m], but rather from the fact that the substituents on the substrate facilitate electron transfer from the substrate to the copper ions, thereby stabilizing the state with an oxidized substrate, that is the Cu^{I}–quinone state. Furthermore, by using the small model from the study by Güell et al.,[5] it was found that the Cu^{II} state was about 10 kcal mol^{-1} lower in energy than the Cu^{I} state, which was found to be the ground state for the fully substituted chemical system, in line with the results for several intermediates (see above), which show that the substituents on the substrate stabilize its oxidation. Thus, the product of the entire reaction, as obtained from our calculations, that is, the quinone state (**6**), corresponds to the formal final product of phenol oxidation, with a quinone, a water molecule, and two Cu^{I} complexes. The calculated free-energy profile for the entire reaction is summarized in Figure 2. The triplet state of this intermediate (**6′**, Figure 14) is only 1.5 kcal mol^{-1} higher than the singlet state and corresponds to a state in which a semiquinone is bound to a Cu^{II}–diamine complex.

Conclusion

To shed light on the mechanism for phenol oxidation in the tyrosinase enzyme, several peroxodicopper complexes have earlier been synthesized to mimic the enzymatic dinuclear copper active site after its reaction with molecular oxygen. One such biomimetic dicopper complex, $[Cu_2O_2(N,N'\text{-di-}tert\text{-butylethylenediamine})_2]^{2+}$ ($[Cu_2O_2(DBED)_2]^{2+}$), which wassynthesized by Stack and co-workers,[4g,j,m] was shown to rapidly oxidize 2,4-di-*tert*-butylphenolate at low temperatures. By using the modified hybrid density functional B3LYP* (15% exact exchange), we studied the mechanism for the oxidation of di-*tert*-butylphenolateinto quinone by the $[Cu_2O_2(DBED)_2]^{2+}$ complex. The reaction mechanism was elucidated from the calculated free-energy profile of the entire reaction (Figure 2). One difficulty in the construction of the energy profile in Figure 2 is that the binding energy of the negatively charged phenolate substrate to the positively charged copper complex cannot be accurately calculated by using the currently available computational methods. Therefore, an essential part of the method that was used in this study was to combine the calculated relative energies with the experimentally determined phenolate-binding constant, thus resulting in a reliable energy profile that could explain the experimental observations.

A solution of the $[Cu_2O_2(DBED)_2]^{2+}$ complex was experimentally shown to exist in equilibrium as 95% in the peroxodicopper(II) form and 5% in the O–O-cleaved bis-μ-oxodicopper(III) form.[4g,h,j] The calculations on the fully substituted $[Cu_2O_2(DBED)_2]^{2+}$ complex show that the peroxo form of the complex is more stable than the bis-μ-oxo form and that the barrier for cleavage of the O–O bond is low, which are in good agreement with the experimental observation of an equilibrium that is predominated by the peroxo form. In contrast, if the *tert*-butyl substituents on the copper ligands are replaced by smaller groups in the calculations, such as methyl groups, the bis-μ-oxo form of the complex becomes significantly lower in energy than the peroxo form.

After the addition of di-*tert*-butylphenolate to a solution of $[Cu_2O_2(DBED)_2]^{2+}$ at extreme temperatures (−120 °C), a bis-μ-oxodicopper(III)–phenolate intermediate (complex **A**) was experimentally observed.[4g,j,m] The calculations show that the O–O-cleaved bis-μ-oxodicopper(III) form of the $[Cu_2O_2(DBED)_2]^{2+}$ complex reacts with the phenolate without any barrier to form the experimentally observed complex (**A**). However, the calculations also show that a $[Cu_2O_2(DBED)_2]^{2+}$–phenolate complex with an intact O–O

bond is significantly lower in energy than the experimentally observed bis-μ-oxo complex (**A**). By using the fully substituted chemical systems in the calculations, we showed that the low-lying peroxo–phenolate complex can not be reached, owing to high barriers. However, by using a smaller model, without *tert*-butyl substituents on the phenolate substrate, in the calculations, these high barriers disappear and, therefore, such a model cannot explain why the peroxo–phenolate complex is not observed experimentally.

Intermediate A is experimentally observed to decay into another intermediate (**B**) with a rate that corresponds to a barrier of 11.2 kcal mol^{-1} and a deuterium kinetic isotope effect of 0.83.[4g,j,m] The calculations show that the transformation of complex **A** into complex **B** occurs in two steps: The first step is the formation of a C–O bond between one of the bridging oxygen atoms in the Cu_2O_2 core and one of the ring-carbon atoms in the coordinated phenolate substrate, which corresponds to a two-electron oxidation of the substrate. In the second step, a ring proton on the substrate is transferred onto the second bridging oxygen in the Cu_2O_2 core and an electron is transferred from the substrate onto one of the copper ions. The first step, which destroys the aromaticity of the substrate and has the character of an electrophilic aromatic substitution reaction, is found to be rate limiting with a calculated barrier of 10.7 kcal mol^{-1} and a kinetic isotope effect of 0.90; these values are in good agreement with the experimental values. The second step, which restores the aromaticity of the substrate, has a lower barrier of 8.0 kcal mol^{-1} and results in the formation of a semiquinone that is coordinated to a mixed Cu^{II}/Cu^{I} complex; this complex should correspond to the experimentally observed intermediate **B**. The singlet ground state for the semiquinone complex agrees with the experimental observation that intermediate **B** is EPR silent. Calculations that use smaller models with an unsubstituted substrate give a qualitatively correct description of this reaction step.

The final step in the reaction involves the observation of a third intermediate (complex **C**), which occurs after the addition of an acid to the solution, thereby reproducing the stoichiometry in the tyrosinase reaction.[4m] In the calculations, this reaction step is modeled by the addition of a proton to the bridging hydroxy group, which results in the cleavage of the copper dimer into two monomers. By using the fully substituted chemical system in the calculations, we found that, in this reaction step, the substrate was oxidized into a quinone and coordinated to one of the Cu^{I} ions with unequal Cu–O bond lengths; this result is in agreement with the experimental observation for the structure of complex **C**.[4m] We also found that, by using a small model with an unsubstituted phenolate substrate, this final reaction step yields a different product, in which a semiquinone is coordinated to a Cu^{II} ion. Because the two Cu–O bonds have quite similar lengths in such a compound, this product cannot correspond to the experimentally observed complex (**C**).

Acknowledgements

We thank Sven de Marothy (Stockholm University) for providing the XYZ viewer, which was used to create all of the figures of the molecular models and also to calculate the dispersion effects. This work was also supported by grants from the National Natural Science Foundation of China (Grant No. 21073014) and Y.F.L. is grateful for the financial support from the China Scholarship Council (No. 2010604109).

[1] a) E. I. Solomon, P. Chen, M. Metz, S.-K. Lee, A. E. Palmer, *Angew. Chem.* **2001**, *113*, 4702–4724; *Angew. Chem. Int. Ed.* **2001**, *40*, 4570–4590; b) Y. Matoba, T. Kumagai, A. Yamamoto, H. Yoshitsu, M. Sugiyama, *J. Biol. Chem.* **2006**, *281*, 8981–8990; c) H. Decker, T. Schweikardt, F. Tuczek, *Angew. Chem.* **2006**, *118*, 4658–4663; *Angew. Chem. Int. Ed.* **2006**, *45*, 4546–4550; d) E. I. Solomon, U. M. Sundaram, T. E. Machonkin, *Chem. Rev.* **1996**, *96*, 2563–2606; e) R. L. Jolley, L. H. Evans, N. Makino, H. S. Mason, *J. Biol. Chem.* **1974**, *249*, 335–345; f) D. E. Wilcox, A. G. Porras, Y. T. Hwang, K. Lerch, M. E. Winkler, E. I. Solomon, *J. Am. Chem. Soc.* **1985**, *107*, 4015–4027; g) E. I. Solomon, M. J. Baldwin, M. D. Lowery, *Chem. Rev.* **1992**, *92*, 521–542; h) K. A. Magnus, B. Hazes, H. Ton-That, C. Bonaventura, J. Bonaventura, W. G. J. Hol, *Proteins* **1994**, *19*, 302–309; i) K. E. van Holde, K. I. Miller, H. Decker, *J. Biol. Chem.* **2001**, *276*, 15563–15566; j) T. Klabunde, C. Eicken, J. C. Sacchettini, B. Krebs, *Nat. Struct. Biol.* **1998**, *5*, 1084–1090; k) B. Hazes, K. H. Kalk, W. G. J. Hol, K. A. Magnus, C. Bonaventura, J. Bonaventura, Z. Dauter, *Protein Sci.* **2008**, *2*, 597–619; l) M. E. Cuff, K. I. Miller, K. E. van Holde, W. A. Hendrickson, *J. Mol. Biol.* **1998**, *278*, 855–870; m) H. Decker, R. Dillinger, F. Tuczek, *Angew. Chem.* **2000**, *112*, 1656–1660; *Angew. Chem. Int. Ed.* **2000**, *39*, 1591–1595; n) R. S. Himmelwright, N. C. Eickman, C. D. LuBien, E. I. Solomon, K. Lerch, *J. Am. Chem. Soc.* **1980**, *102*, 7339–7344.

[2] a) S. Itoh, S. Fukuzumi, *Acc. Chem. Res.* **2007**, *40*, 592–600; b) P. E. M. Siegbahn, *J. Biol. Inorg. Chem.* **2003**, *8*, 567–576; c) M. E. Winkler, K. Lerch, E. I. Solomon, *J. Am. Chem. Soc.* **1981**, *103*, 7001–7003; d) T. Inoue, Y. Shiota, K. Yoshizawa, *J. Am. Chem. Soc.* **2008**, *130*, 16890–16897; e) T. Osako, K. Ohkubo, M. Taki, Y. Tachi, S. Fukuzumi, S. Itoh, *J. Am. Chem. Soc.* **2003**, *125*, 11027–11033; f) R. P. Ferrari, E. Laurenti, E. M. Ghibaudi, L. Casella, *J. Inorg. Biochem.* **1997**, *68*, 61–69; g) J. W. Ginsbach, M. T. Kieber-Emmons, R. Nomoto, A. Noguchi, Y. Ohnishi, E. I. Solomon, *Proc. Natl. Acad. Sci. USA* **2012**, *109*, 10793–10797; h) P. E. M. Siegbahn, T. Borowski, *Faraday Discuss.* **2011**, *148*, 109–117.

[3] a) A. L. Gavrilova, B. Bosnich, *Chem. Rev.* **2004**, *104*, 349–384; b) S. K. Das, D. Biswas, R. Maiti, S. Sarkar, *J. Am. Chem. Soc.* **1996**, *118*, 1387–1397; c) H. Sugimoto, H. Tsukube, *Chem. Soc. Rev.* **2008**, *37*, 2609–2619; d) Y.-F. Liu, R.-Z. Liao, W.-J. Ding, J.-G. Yu, R.-Z. Liu, *J. Biol. Inorg. Chem.* **2011**, *16*, 745–752; e) E. A. Lewis, W. B. Tolman, *Chem. Rev.* **2004**, *104*, 1047–1076; f) L. M. Mirica, X. Ottenwaelder, T. D. P. Stack, *Chem. Rev.* **2004**, *104*, 1013–1046; g) C. X. Zhang, H.-C. Liang, K. J. Humphreys, K. D. Karlin, in *Advances in Catalytic Activation of Dioxygen by Metal Complexes Vol. 26* (Ed.: L. I. Simándi), Kluwer Academic, Dordrecht, **2003**, pp. 79–121; h) K. D. Karlin, A. D. Zuberbühler in *Bioinorganic Catalysis*, 2nd ed. (Eds.: J. Reedijk, E. Bouwman), Marcel Dekker, New York, **1999**, pp. 469–543; i) K. D. Karlin, S. Kaderli, A. D. Zuberbühler, *Acc. Chem. Res.* **1997**, *30*, 139–147; j) K. D. Karlin, Y. Gultneh in *Progress in Inorganic Chemistry*, John Wiley & Sons, **2007**, pp. 219–327; k) L. Q. Hatcher, K. D. Karlin, *J. Biol. Inorg. Chem.* **2004**, *9*, 669–683; l) G. Battaini, A. Granata, E. Monzani, M. Gullotti, L. Casella in *Advances in Inorganic Chemistry, Vol. 58* (Eds.: R. v. Eldik, J. Reedijk), Academic Press, Amsterdam, **2006**, pp. 185–233; m) L. Que, W. B. Tolman, *Nature* **2008**, *455*, 333–340; n) A. De, S. Mandal, R. Mukherjee, *J. Inorg. Biochem.* **2008**, *102*, 1170–1189; o) C. Citek, C. T. Lyons, E. C. Wasinger, T. D. P. Stack, *Nat. Chem.* **2012**, *4*, 317–322.

[4] a) E. Pidcock, H. V. Obias, C. X. Zhang, K. D. Karlin, E. I. Solomon, *J. Am. Chem. Soc.* **1998**, *120*, 7841–7847; b) D. Ghosh, R. Mukher-

jee, *Inorg. Chem.* **1998**, *37*, 6597–6605; c) L. Santagostini, M. Gullotti, E. Monzani, L. Casella, R. Dillinger, F. Tuczek, *Chem. Eur. J.* **2000**, *6*, 519–522; d) S. Itoh, H. Kumei, M. Taki, S. Nagatomo, T. Kitagawa, S. Fukuzumi, *J. Am. Chem. Soc.* **2001**, *123*, 6708–6709; e) L. M. Mirica, M. Vance, D. J. Rudd, B. Hedman, K. O. Hodgson, E. I. Solomon, T. D. P. Stack, *J. Am. Chem. Soc.* **2002**, *124*, 9332–9333; f) S. P. Foxon, D. Utz, J. Astner, S. Schindler, F. Thaler, F. W. Heinemann, G. Liehr, J. Mukherjee, V. Balamurugan, D. Ghosh, R. Mukherjee, *Dalton Trans.* **2004**, 2321–2328; g) L. M. Mirica, M. Vance, D. J. Rudd, B. Hedman, K. O. Hodgson, E. I. Solomon, T. D. P. Stack, *Science* **2005**, *308*, 1890–1892; h) L. M. Blomberg, M. R. A. Blomberg, P. E. M. Siegbahn, *J. Inorg. Biochem.* **2005**, *99*, 949–958; i) S. Palavicini, A. Granata, E. Monzani, L. Casella, *J. Am. Chem. Soc.* **2005**, *127*, 18031–18036; j) L. M. Mirica, D. J. Rudd, M. A. Vance, E. I. Solomon, K. O. Hodgson, B. Hedman, T. D. P. Stack, *J. Am. Chem. Soc.* **2006**, *128*, 2654–2665; k) L. Li, A. A. N. Sarjeant, K. D. Karlin, *Inorg. Chem.* **2006**, *45*, 7160–7172; l) O. Sander, A. Henß, C. Näther, C. Würtele, M. C. Holthausen, S. Schindler, F. Tuczek, *Chem. Eur. J.* **2008**, *14*, 9714–9729; m) B. T. Op′t Holt, M. A. Vance, L. M. Mirica, D. E. Heppner, T. D. P. Stack, E. I. Solomon, *J. Am. Chem. Soc.* **2009**, *131*, 6421–6438; n) M. Rolff, J. Schottenheim, H. Decker, F. Tuczek, *Chem. Soc. Rev.* **2011**, *40*, 4077–4098; o) P. L. Holland, K. R. Rodgers, W. B. Tolman, *Angew. Chem.* **1999**, *111*, 1210–1213; *Angew. Chem. Int. Ed.* **1999**, *38*, 1139–1142; p) K. D. Karlin, J. C. Hayes, Y. Gultneh, R. W. Cruse, J. W. McKown, J. P. Hutchinson, J. Zubieta, *J. Am. Chem. Soc.* **1984**, *106*, 2121–2128.

[5] M. Güell, J. Luis, M. Solà, P. Siegbahn, *J. Biol. Inorg. Chem.* **2009**, *14*, 229–242.

[6] a) S. Grimme, *J. Comput. Chem.* **2004**, *25*, 1463–1473; b) S. Grimme, *J. Comput. Chem.* **2006**, *27*, 1787–1799; c) P. E. M. Siegbahn, M. R. A. Blomberg, S.-L. Chen, *J. Chem. Theory Comput.* **2010**, *6*, 2040–2044.

[7] P. Comba, B. Martin, A. Muruganantham, J. Straub, *Inorg. Chem.* **2012**, *51*, 9214–9225.

[8] J. S. Woertink, L. Tian, D. Maiti, H. R. Lucas, R. A. Himes, K. D. Karlin, F. Neese, C. Würtele, M. C. Holthausen, E. Bill, J. r. Sundermeyer, S. Schindler, E. I. Solomon, *Inorg. Chem.* **2010**, *49*, 9450–9459.

[9] a) C. Lee, W. Yang, R. G. Parr, *Phys. Rev. B* **1988**, *37*, 785; b) P. J. Stephens, F. J. Devlin, C. F. Chabalowski, M. J. Frisch, *J. Phys. Chem.* **1994**, *98*, 11623–11627; c) M. Reiher, O. Salomon, B. A. Hess, *Theor. Chem. Acc.: Theory, Computation, and Modeling (Theor. Chim. Acta)* **2001**, *107*, 48–55; d) A. D. Becke, *Phys. Rev. A:* **1988**, *38*, 3098–3100; e) A. D. Becke, *J. Chem. Phys.* **1993**, *98*, 1372–1377; f) A. D. Becke, *J. Chem. Phys.* **1993**, *98*, 5648–5652.

[10] a) P. E. M. Siegbahn, M. R. A. Blomberg, *Ann. Pharm. Belg. Ann. Rev. Phys. Chem.* **1999**, *50*, 221–249; b) O. Salomon, M. Reiher, B. A. Hess, *J. Chem. Phys.* **2002**, *117*, 4729–4737; c) L. A. Curtiss, K. Raghavachari, P. C. Redfern, J. A. Pople, *J. Chem. Phys.* **2000**, *112*, 7374–7383.

[11] E. Rezabal, J. Gauss, J. M. Matxain, R. Berger, M. Diefenbach, M. C. Holthausen, *J. Chem. Phys.* **2011**, *134*, 064304.

[12] Jaguar, Schrodinger, LLC, New York, **2007**, version 7.0.

[13] P. J. Hay, W. R. Wadt, *J. Chem. Phys.* **1985**, *82*, 299–310.

[14] a) J. Thom, H. Dunning, *J. Chem. Phys.* **1989**, *90*, 1007–1023; b) R. A. Kendall, J. Thom, H. Dunning, R. J. Harrison, *J. Chem. Phys.* **1992**, *96*, 6796–6806; c) D. E. Woon, J. Thom, H. Dunning, *J. Chem. Phys.* **1993**, *98*, 1358–1371.

[15] a) D. J. Tannor, B. Marten, R. Murphy, R. A. Friesner, D. Sitkoff, A. Nicholls, B. Honig, M. Ringnalda, W. A. Goddard, *J. Am. Chem. Soc.* **1994**, *116*, 11875–11882; b) B. Marten, K. Kim, C. Cortis, R. A. Friesner, R. B. Murphy, M. N. Ringnalda, D. Sitkoff, B. Honig, *J. Phys. Chem.* **1996**, *100*, 11775–11788.

[16] Gaussian 09, Revision B.01, M. J. Frisch, G. W. Trucks, H. B. Schlegel, G. E. Scuseria, M. A. Robb, J. R. Cheeseman, G. Scalmani, V. Barone, B. Mennucci, G. A. Petersson, H. Nakatsuji, M. Caricato, X. Li, H. P. Hratchian, A. F. Izmaylov, J. Bloino, G. Zheng, J. L. Sonnenberg, M. Hada, M. Ehara, K. Toyota, R. Fukuda, J. Hasegawa, M. Ishida, T. Nakajima, Y. Honda, O. Kitao, H. Nakai, T. Vreven, J. A. Montgomery, Jr., J. E. Peralta, F. Ogliaro, M. Bearpark, J. J. Heyd, E. Brothers, K. N. Kudin, V. N. Staroverov, R. Kobayashi, J. Normand, K. Raghavachari, A. Rendell, J. C. Burant, S. S. Iyengar, J. Tomasi, M. Cossi, N. Rega, J. M. Millam, M. Klene, J. E. Knox, J. B. Cross, V. Bakken, C. Adamo, J. Jaramillo, R. Gomperts, R. E. Stratmann, O. Yazyev, A. J. Austin, R. Cammi, C. Pomelli, J. W. Ochterski, R. L. Martin, K. Morokuma, V. G. Zakrzewski, G. A. Voth, P. Salvador, J. J. Dannenberg, S. Dapprich, A. D. Daniels, Ö. Farkas, J. B. Foresman, J. V. Ortiz, J. Cioslowski, D. J. Fox, Gaussian, Inc., Wallingford CT, **2009**.

Received: August 28, 2012
Published online: January 4, 2013

